The structure of water in the hydration shell of cations from x-ray Raman and small angle x-ray scattering measurements

ARTICLE *in* THE JOURNAL OF CHEMICAL PHYSICS · FEBRUARY 2011

Impact Factor: 2.95 · DOI: 10.1063/1.3533958 · Source: PubMed

The structure of water in the hydration shell of cations from x-ray Raman and small angle x-ray scattering measurements

Iradwikanari Waluyo,[1,2] Congcong Huang,[2] Dennis Nordlund,[2] Uwe Bergmann,[3] Thomas M. Weiss,[2] Lars G. M. Pettersson,[4] and Anders Nilsson[2,4,a)]
[1]*Department of Chemistry, Stanford University, Stanford, California 94305, USA*
[2]*Stanford Synchrotron Radiation Lightsource, SLAC National Accelerator Laboratory, P.O. Box 20450, Stanford, California 94309, USA*
[3]*Linac Coherent Light Source, SLAC National Accelerator Laboratory, P.O. Box 20450, Stanford, California 94309, USA*
[4]*Department of Physics, AlbaNova University Center, Stockholm University, SE-106 91 Stockholm, Sweden*

(Received 21 September 2010; accepted 15 December 2010; published online 14 February 2011)

X-ray Raman scattering (XRS) spectroscopy and small angle x-ray scattering (SAXS) are used to study water in aqueous solutions of NaCl, $MgCl_2$, and $AlCl_3$ with the particular aim to provide information about the structure of the hydration shells of the cations. The XRS spectra show that Na^+ weakens the hydrogen bonds of water molecules in its vicinity, similar to the effect of increased temperature and pressure. Mg^{2+} and Al^{3+}, on the other hand, cause the formation of short and strong hydrogen bonds between the surrounding water molecules. The SAXS data show that Mg^{2+} and Al^{3+} form tightly bound hydration shells that give a large density contrast in the scattering data. From the form factors extracted from the SAXS data, we found that Mg^{2+} and Al^{3+} have, respectively, an equivalent of one and one and a half stable hydration shells that appear as a density contrast. In addition, we estimated that the density of water in the hydration shells of Mg^{2+} and Al^{3+} is, respectively, ~61% and ~71% higher than in bulk water. © *2011 American Institute of Physics*. [doi:10.1063/1.3533958]

I. INTRODUCTION

The interaction between solvated ions and water has been a subject of great interest due to its importance in various chemical, biological, and environmental processes. Various experimental and theoretical studies have explored aqueous solutions of ions, both in the bulk[1,2] and at interfaces.[3,4] In the 19th century, Franz Hofmeister observed that different salts influence protein precipitation in different ways.[5] It is now believed that this so-called "Hofmeister effect" is due to the ability of ions to either increase or decrease the ordering of the surrounding water molecules.[2] Ion size has been shown to be correlated to the ability to bind water tightly; smaller ions with high charge densities tend to be structure makers while larger ions with lower charge densities are generally structure breakers.[6,7] This classification has been derived from measurements of macroscopic properties such as viscosity[8,9] and hydration entropy.[10] The relative strength of ion–water interaction has been quantified through size-exclusion chromatography to determine the apparent dynamic hydration numbers, i.e., the number of water molecules bound to an ion as it elutes through the chromatographic column.[11] The results generally agree that ions with higher charge density have higher numbers of tightly bound water molecules. This has also been proposed as the mechanism behind cellular ion channels being closed to strongly hydrated Na^+ ions while allowing formally larger, but more easily dehydrated, K^+ ions to pass through.[12–15]

While the relative strengths of the direct interaction between different ions and water molecules in the first hydration shell are well understood, the effect of ions on the hydrogen (H-) bonding of water beyond the first hydration shell is still debated despite extensive research. The classification of ions as structure breakers or structure makers can even be misleading in this regard. A Monte Carlo study by Hribar *et al.*, for example, proposed that small ions interact with water molecules through strong electrostatic interaction accompanied by H-bond breaking while large ions that interact weakly with water facilitate the formation of H-bonds.[7] Neutron diffraction studies have suggested that monovalent ions have a pressurelike effect on water that extends beyond the first hydration shell.[16] However, it is unclear whether the effect on the second shell can be directly observed from the experimental data or whether it arises from the empirical potential structure refinement (EPSR) simulation model.[17] The pressurelike effect has been confirmed for NaCl solutions in a molecular dynamics study of the self-diffusion coefficient of water, which reflects the mobility of water molecules.[18] Ultrafast vibrational pump-probe spectroscopy,[19,20] on the other hand, proposed that ions only influence water molecules in the first hydration shell (i.e., in direct contact with the ion). More recently, a combined experimental study using dielectric spectroscopy and femtosecond infrared spectroscopy revealed that there is a cooperativity effect between cations and anions in the structuring of the water molecules in the solution and that in some solutions the effect of the ions extends beyond the first hydration shell.[21]

a)Author to whom correspondence should be addressed. Electronic mail: nilsson@slac.stanford.edu.

Multivalent cations such as Mg^{2+} and Al^{3+}, in particular, are considered as strongly interacting with water molecules in their hydration shells due to their high charge density. The structure of the first hydration shell of Mg^{2+}, Al^{3+}, and a variety of other cations has been extensively characterized experimentally using neutron diffraction, x-ray diffraction, and extended x-ray absorption fine structure spectroscopy as well as theoretically using molecular dynamics simulations (for a comprehensive review, see Ref. 1). Infrared spectroscopy analyzed using a double-difference method shows that Mg^{2+} and Al^{3+} form, respectively, at least one and two well-defined hydration shells.[22,23] However, the observation of distinct O–D stretch bands corresponding to H-bonds between first and second hydration shells for Mg^{2+}, as well as between second and third hydration shells for Al^{3+} (Refs. 22 and 23), indicates that at least one more hydration shell is present for each cation.

X-ray absorption spectroscopy (XAS) is an element-sensitive technique for studying the unoccupied states of a molecule, which has been shown to provide a sensitive probe for various hydrogen (H-) bonding environments in water.[24–28] A 2004 study by Wernet *et al*. proposed that liquid water is predominantly comprised of asymmetrically (distorted) H-bonded water molecules with a smaller population of tetrahedrally H-bonded water species, in direct contrast to the conventional tetrahedral picture of water.[26] This was based on temperature dependent measurements and using various model systems such as bulk and surface of thin film of ice in a controlled ultrahigh vacuum environment and later verified in additional experimental studies.[27,28] This interpretation is also supported by theoretical XAS calculations,[24–26,29,30] but other means to theoretically interpret the experimental data have also been put forward and discussed.[31–35] Although there is a debate regarding the quantitative interpretation, we can conclude that XAS is a reliable method for detecting changes (i.e., weakening or strengthening) in the H-bonding network of water, for example, due to temperature (for further details, see Ref. 27). In addition, XAS has been utilized to probe the electronic structure of hydrated cations in aqueous solutions.[36,37] However, results from XAS measurements of water in aqueous solutions of ions have so far yielded conflicting interpretations. Total electron yield XAS studies by Cappa *et al*. proposed that XAS spectral changes are caused by direct electronic perturbation by the anions on the surrounding water molecules while monovalent cations have no significant effect on the structure of water and divalent cations affect water structures through charge transfer;[38,39] however, the spectrum calculations used for the analysis have been disputed (see discussion in Ref. 29). The fluorescence yield (FY) XAS study by Näslund *et al*., on the other hand, concluded that anions do not affect the electronic structure of the water molecules and that changes in the XAS spectra are instead caused by the reorganization of H-bonding among the water molecules near the cations;[40] the effect of anions, such as Cl^-, on the spectrum can be shown to simply reflect the longer H-bond distance of H_2O–Cl^- compared to H_2O–H_2O.[41]

In the present work, we use x-ray Raman scattering (XRS) and small-angle x-ray scattering (SAXS) to probe water structure in solutions of NaCl, $MgCl_2$, and $AlCl_3$. These salts were selected to systematically study the effect of increasing charge, and by extension, decreasing size and increasing charge density, of the cations. XRS is a hard x-ray alternative to XAS in which a high-energy photon (∼7 keV) is inelastically scattered and a fraction of the energy is used to excite a core electron to an unoccupied orbital corresponding to an x-ray absorption process. XRS does not suffer from saturation effects and sample handling is much simpler since it does not require a vacuum environment. Momentum transfers within the dipole limit can be selected to satisfy the dipole selection rule of the normal XAS process.[42–44] XRS has been used to study liquid water in various conditions, such as temperature dependence,[26,27,45] pressure dependence,[46] isotopic substitution,[27,47] and confinement in reverse micelles.[48] Recent instrumental developments have improved the energy resolution of XRS measurements from ∼1 to ∼0.5 eV.[27,45]

SAXS is a sensitive probe for density variations in liquid samples. The presence of structures, instantaneous or static, giving rise to density inhomogeneities will lead to an extra scattering intensity at small momentum transfers;[49] note that the scattering occurs on an attosecond time scale leading to the SAXS signal resulting from basically frozen structures. A wealth of information can be extracted from the SAXS scattering curve, such as the size of and the separation between such structures as well as the electron density difference relative to the surrounding medium. In a recent study, SAXS, in combination with XAS and x-ray emission spectroscopy (XES), was used to detect density fluctuations in bulk water analyzed as due to fluctuations between two distinct local structures in liquid water even at ambient conditions.[45] These were interpreted to correspond to the dominant distorted (or asymmetric) H-bonded species in XAS and XES spectra and tetrahedrally H-bonded water molecules giving rise to instantaneous regions of, respectively, high-density liquid (HDL) and low-density liquid water (LDL).[45] These two structures were proposed to continuously interconvert, resulting in a temperature dependent equilibrium with the ratio determined by the given temperature; as the temperature of the system is increased, a shift in the balance from the LDL to the HDL structure is observed, accompanied by increasing disorder of the HDL species.[45,50] Although this interpretation is currently under debate,[51–53] recent SAXS data of supercooled H_2O and D_2O (Ref. 54) provide support for a picture of critical fluctuations between two liquid local states being enhanced as a transition is approached in the deeply supercooled regime. In the present work, we will apply these techniques to elucidate the details of how ions affect the balance between strongly H-bonded and disordered local water structures.

II. EXPERIMENTAL DETAILS

NaCl (1 and 4 M), $MgCl_2$ (1 and 2.8 M), and $AlCl_3$ (1 and 2.8 M) solutions were prepared using commercially obtained salts without further preparations (NaCl and $MgCl_2 \cdot 6H_2O$ > 99% from Fisher Chemical and $AlCl_3 \cdot 6H_2O$ 99% from Acros Organics) dissolved in Millipore-purified H_2O (∼18 MΩ cm). XRS measurements were performed at

the Stanford Synchrotron Radiation Lightsource (SSRL) at the hard x-ray beamline (BL) 6–2 equipped with a Si(311) double crystal monochromator. The experiments were done in two separate runs (NaCl and $AlCl_3$ in one run and $MgCl_2$ in a separate run). The spectra of pure water measured in both runs were identical within statistical error bars, confirming the reliability and reproducibility of XRS demonstrated in a previous study.[47] The experimental setup was identical for both runs; the only difference was the synchrotron ring current (100 mA for $MgCl_2$ and 200 mA for NaCl and $AlCl_3$), which only influenced the photon flux and, consequently, count rate and measurement time.

Raman scattering at ~45° scattering angle was analyzed using a high-energy-resolution multicrystal spectrometer consisting of 14 Si (440) analyzer crystals with a diameter of 100 mm in a Rowland geometry (1 m radius) and fixed Bragg angle of 88°. The setup selects 6.46 keV photons with an energy resolution of ~0.5 eV and momentum transfers of $Q = 2.6 \pm 1$ Å^{-1}. The monochromator energy was scanned from 6980 to 7032 eV (corresponding to energy transfers of ~520 to 572 eV) with a flux of ~2.5×10^{12} photons/s (for the NaCl and $AlCl_3$ runs) and ~0.8×10^{12} photons/s (for the $MgCl_2$ run) and a focused beam spot size of ~0.1×1 mm^2. The overall energy resolution amounted to 0.55 ± 0.02 eV full width at half maximum. The energy scale was calibrated by recording the elastic peak every five scans. The sample was placed in a 60 mL polyethylene bottle with a Si_3N_4 membrane (5×5 mm^2 area and 1 μm thickness) as the x-ray window. Beam damage was avoided by keeping the sample moving continuously using a Teflon-coated magnetic stirring bar inside the bottle and a magnetic stir plate. The x-ray path from the beam pipe to the detector (including the sample) was kept in 1 atm He to avoid background scattering from air. A Vortex single element Si drift detector was used in photon counting mode with an electronic window centered at ~6460 eV to reduce the background signal.

The SAXS measurements were performed at the BioSAXS beamline (BL) 4–2 at SSRL using a beam energy of 11 keV and an optical fiber coupled CCD detector (MarCCD165). The capillary sample holder with a diameter of 1.5 mm was integrated into the vacuum setup eliminating the need for additional windows between the beam defining slit and the exit window of the flight path. The sample holder, detector, and the path in between were placed in a vacuum of 1×10^{-3} Torr in order to reduce the background scattering. The sample device was connected to a constant temperature bath, within which water was circulated to maintain and control the sample temperature. The scattering vector is defined as $Q = 4\pi \sin\theta/\lambda$, where λ is the wavelength and θ is one half of the scattering angle. In order to reduce the possibility of radiation damage, the data were continuously collected for 10 frames with 1 min each and all scattering images were averaged afterward. The scattering curves have been corrected for the primary beam intensity, absorption, and detector readout noise. The scattering of the empty capillary, observed to contribute ~20% of the total scattering at Q > 0.05 Å^{-1}, was measured separately and subtracted from the total scattering signal.

III. RESULTS AND DISCUSSION

A. X-ray Raman scattering

Figure 1(a) displays the O 1*s* XRS spectra of water in NaCl solution at 1 M (red) and 4 M (blue) concentration compared with the spectrum of pure bulk water (black). The O 1*s* XRS spectrum of water is generally divided into three regions: pre-edge (535 eV), which is sensitive to weak/distorted H-bonds; main-edge (537–538 eV), which is also mostly sensitive to weak H-bonds but in addition contains contributions from strong H-bonds, and the post-edge (540–541 eV), which corresponds to strong/intact H-bonds.[24,25,27] The presence of NaCl results in an increase of the pre- and main-edge and decrease of the post-edge, and the effect is enhanced with increased concentration, suggesting that the fraction of more weakly H-bonded water molecules (i.e., HDL species[45]) has increased. This observation agrees with the previously published FY-XAS spectra of NaCl.[40] At first glance, the general trend of the spectral changes, shown in the difference spectra [top of Fig. 1(a)], i.e., the spectra of aqueous solutions minus the spectrum of pure water, seems similar to the changes caused by a temperature increase (i.e., intensity redistribution

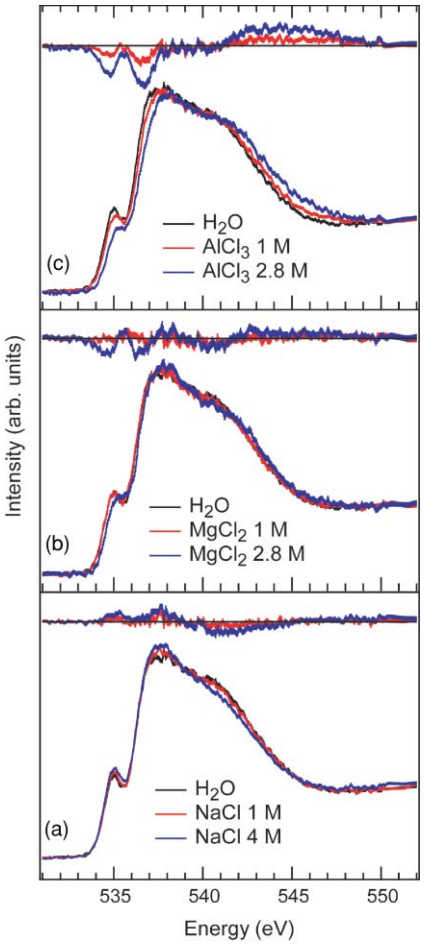

FIG. 1. O 1*s* XRS spectra of (a) NaCl (red: 1 M, blue: 4 M), (b) $MgCl_2$(red: 1 M, blue: 2.8 M), and (c) $AlCl_3$ (red: 1 M, blue: 2.8 M) solutions compared with pure water (black). The difference spectra, obtained by subtracting the spectrum of pure water from the solutions, are displayed above each set of spectra.

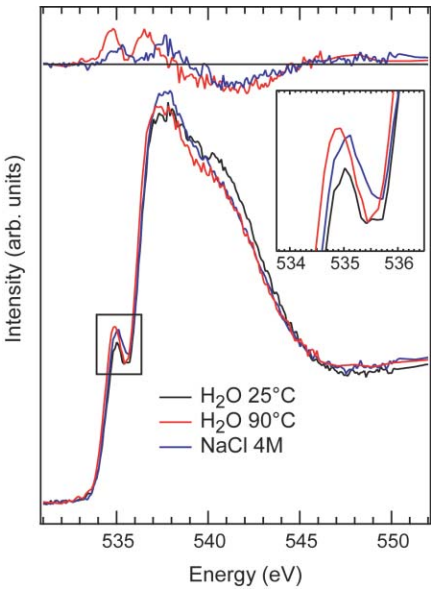

FIG. 2. O 1*s* XRS spectra of pure water at 25 °C (black) compared with pure water at 90 °C (red, from Ref. 27) and 4 M NaCl solution. The difference spectra between 90 °C water and 25 °C water (red) and 4 M NaCl and 25 °C water (blue) are displayed at the top. The inset shows the enlarged pre-edge region.

from the post-edge to the pre- and main-edge).[45] However, upon closer inspection, a significant difference can be observed between the effect of temperature increase and NaCl solvation.

Figure 2 shows the spectra of pure liquid water (black) and 4 M NaCl (blue) at 25 °C compared with the spectrum of liquid water at 90 °C (from Ref. 45), with the difference spectra (90 °C H_2O–25 °C H_2O in red and 4 M NaCl–25 °C H_2O in blue) displayed at the top. An enlarged view of the pre-edge peak (inset of Fig. 2) clearly displays that, although the intensity of the pre-edge peaks of 90 °C H_2O and 4 M NaCl both increase relative to 25 °C H_2O, the peak position of 90 °C H_2O also shifts to lower energy while that of 4 M NaCl is unshifted compared to 25 °C H_2O. In hot water, the pre-edge shift toward lower energy (i.e., closer to the gas-phase position) has been interpreted as due to the increased disorder in the H-bond distorted (HDL) species of water through thermal excitation as the temperature of the system is increased, while the intensity redistribution from the post-edge to the pre- and main-edge is a signature of H-bond weakening (i.e., conversion from LDL to HDL).[45] However, in the case of NaCl solvation, H-bonds are weakened or distorted without introducing additional thermal energy to the system, consistent with the increased pre-edge being located at the same energy position as at 25 °C H_2O. The conversion from LDL to HDL species is also consistent with the expected effects of pressure increase, in agreement with the conclusions of Mancinelli *et al.*[16]

The XRS spectra of 1 and 2.8 M $MgCl_2$ and $AlCl_3$ are compared with the spectrum of pure water (black) in Figs. 1(b) and 1(c), respectively. By replacing the Na^+ cation with Mg^{2+} and Al^{3+}, we can investigate the effect of increasing charge density of the cation. In Fig. 1(b), the difference between 1 M $MgCl_2$ and H_2O is very small. However, at higher concentration, the spectral changes become more apparent, namely the pre-edge becomes less well defined and the entire spectrum is shifted by 0.14 eV although the intensity ratio between pre- and post-edge only changes slightly from pure water. For $AlCl_3$ solutions, shown in Fig. 1(c), the changes are already visible at 1 M concentration and strongly enhanced at 2.8 M. In addition to the shift to higher energy (~0.1 eV for 1 M $AlCl_3$ and ~0.3 eV for 2.8 M $AlCl_3$), a decrease in the pre-edge intensity is observed along with an increase in the post-edge region. The XRS spectra of the $AlCl_3$ solutions, and the absence of any features due to OH^- species that could result from hydrolysis, are consistent with the published FY-XAS spectra of the same sample.[40]

According to the "bond-length-with-a-ruler" concept,[55–57] the energy position of a σ^* shape resonance depends on the bond length. The σ^* shape resonance appears when a low energy photoelectron is briefly trapped in a molecular potential barrier before leaving the system. In a molecular orbital picture, the electron is excited into an unoccupied orbital with an antibonding character located above the ionization potential. Although the dependence of the shape resonance energy position on bond length has been disputed,[58] the bond-length-with-a-ruler concept has been supported by various experimental results[56,57,59] as well as results from *ab initio* calculations of various hydrocarbon molecules where it was shown that the energy position of the σ^* shape resonance is shifted to higher energy as the C–C bond length decreases.[60] Although the free water molecule, unlike other molecules such as O_2, N_2, C_2H_2, etc., does not have a shape resonance,[55] in the condensed phase such as liquid water and ice, the formation of H-bonds gives rise to a set of new molecular orbitals[61] due to orbital mixing in addition to electrostatic attraction. The states corresponding to the post-edge excitation have been shown to have an antibonding character, and the post-edge can, therefore, be considered as a shape resonance whose energy position depends on H-bond distance as concluded from both experimental and computational observations.[27,30]

Theoretical simulations have shown that as the H-bond distance of ice is elongated, the post-edge peak is shifted to lower energy and the same effect can be expected also for water.[30] In addition, experimental FY-XAS data of HCl solutions have shown that at high concentrations, in which the protonated water predominantly exists in the Eigen form (H_3O^+) with significantly shorter H-bond distance compared to pure water, a shift of the post-edge to higher energy is observed accompanied by a decreased pre-edge and increased post-edge.[62] The spectrum of 2.8 M $AlCl_3$ solution, in fact, resembles the spectrum of 6 M HCl solution, although a direct comparison is difficult since the spectra were measured using different methods. $AlCl_3$ solutions can undergo hydrolysis, producing an acidic solution. However, relatively high concentrations (i.e., 4 and 6 M) of HCl are required to obtain spectral changes related to short H-bonds due to the presence of the Eigen species of protonated water,[62] while the spectral changes in $AlCl_3$ solutions are already observable at relatively low concentrations (i.e., 0.5 M, not shown). In addition, for strongly hydrolyzed solutions such as $FeCl_3$, a peak at 530–532 eV (below the pre-edge) appears due to the presence of

hydroxyl groups,[63] which is not observed for the spectra of $AlCl_3$ solutions. Therefore, the presence of protonated water in $AlCl_3$ solutions cannot account for these spectral changes. The addition of $AlCl_3$, and to a lesser extent $MgCl_2$, to water, thus, causes the formation of shorter (and, therefore, stronger) H-bonds in water.

The observation that $MgCl_2$ and $AlCl_3$ solvation induces changes to the XRS spectra in the opposite way from NaCl is already an indication that the multivalent cations Mg^{2+} and Al^{3+} affect water structure differently from the monovalent Na^+ cation. Since all O atoms in the sample contribute equally to the absorption intensity, XRS cannot distinguish water in the hydration shells of the ions and water molecules outside the hydration shells. As relatively high concentrations are required to clearly see the spectral changes, we can assume that only water molecules in close proximity of the ions are affected. However, since H-bonding is probed, our data concern water–water interactions, likely between the first and second hydration shells, and not simply ion–water interaction.

In earlier work by Cappa *et al.*,[38,39] the spectral changes were assigned as due to distortions of the unoccupied states of water in the field of the cation and the role of charge transfer from water to the cation was emphasized. However, charge transfer from, or orbital mixing involving, occupied valence levels should lead to absorption at lower energy (below the pre-edge) corresponding to valence transitions rather than transitions into higher excited states. Such transitions are indeed observed in the hydration sphere of open-3*d*-shell transition metals[63] and in dative bonding involving the oxygen lone-pair in water binding through the oxygen to a Pt(111) surface,[64] but not in the case of closed-shell ions even as highly charged as Al^{3+}.[63] There is thus no experimental indication of the proposed mechanism as actually also noted by Cappa *et al.*[39] when they find computed intensity around 532 eV in their models of solvated Mg^{2+}, however, without realizing the implications for their interpretation.

Before discussing in depth the effect of the cations, we must first consider the role of the Cl^- anion. X-ray and neutron diffraction studies, as well as molecular dynamics simulations, have determined that on average six water molecules comprise the first hydration shell of Cl^- with a Cl–O distance of ∼3.15 Å and Cl–O–H angle of less than 12°.[1] With an almost linear Cl–O–H angle, Cl^- is located at roughly the same position as an acceptor O atom in bulk water, only at a longer distance.[65] Therefore, Cl^- ions can fit into the H-bonding network of water without any significant restructuring of the H-bonding of the surrounding water molecules. However, the longer Cl–O distance (∼3.15 Å) compared to the O–O distance in bulk water (∼2.8 Å) must be considered in the interpretation of the XRS spectra according to the bond-length-with-a-ruler principle described previously. In Ref. 30, it was shown that asymmetrically increasing a donating H-bond distance not only shifts the post-edge to lower energy but also induces an increased intensity in the pre- and main-edge regions, as is also observed in Fig. 1(a). However, the spectra of $MgCl_2$ and $AlCl_3$ do not show the expected effect of H-bond elongation by Cl^- although there are more Cl^- ions for the same concentration compared to for NaCl. This indicates that the effect of Cl^- may actually be small and does not completely account for the spectral changes in Fig. 1(a). Therefore, the observed increase in the HDL population is likely caused by Na^+. Note that the spectrum calculations by Cappa *et al.*[38] comparing computed spectra of water donating an H-bond either to Cl^- or to another water were in both cases performed at 2.818 Å which in the case of Cl^- gives strong Pauli repulsion with ensuing artificial distortions of the electronic structure of the water molecule due to the nearly 0.3 Å too short distance.

The interpretation for Mg^{2+} and Al^{3+} is even more obvious and the increased fraction of shorter and stronger H-bonds suggests that the effect of the cations is much greater and the effect of Cl^- can be assumed to be negligible. Therefore, it can be concluded that the increased fraction of strongly H-bonded water is caused by the presence of Mg^{2+} and Al^{3+}, with the latter having a stronger effect. This is in agreement with data from various x-ray diffraction and molecular dynamics studies that determined that the water O–O distances between the first and second shells of Mg^{2+} and Al^{3+} are shorter than in bulk water (an average of ∼2.66 Å for Al^{3+} and ∼2.71 Å for Mg^{2+}, compared to 2.8 Å in bulk water).[1,66–69]

At high concentrations, solvated ions are known to form ion pairs (see, e.g., Ref. 70 for Na–Cl ion pairing). In addition, the strength of the ion pairing between acetate and various cations (Na^+, Li^+, K^+, and NH_4^+) was found to follow the Hofmeister series except for Li^+.[71] Therefore, assuming that Na^+, Mg^{2+}, and Al^{3+} ions follow a similar trend, then the strength of the ion pair interaction is expected to be $Al^{3+} > Mg^{2+} > Na^+$. The XAS spectra were measured at relatively high concentrations (i.e., 4 M for NaCl and 2.8 M for $MgCl_2$ and $AlCl_3$), where ion pairs are likely formed. However, the trends in the difference spectra at high concentrations are consistent with those at lower concentrations (e.g., 1 M); therefore, the ion pairs at high concentrations likely have insignificant effects on the XAS spectra.

B. Small angle x-ray scattering

The SAXS data for NaCl, $MgCl_2$, and $AlCl_3$ solutions at various concentrations (solid curves) compared to pure water (dashed curve) are displayed in Fig. 3 where the scattering intensity $I(Q)$ is plotted as a function of momentum transfer Q (note the different intensity scales between the three figures). For NaCl solutions [Fig. 3(a)], other than the increase of the scattering intensity as more ions are solvated, the overall shape of the scattering curve closely resembles that of pure liquid water. The absence of any notable features in the scattering curve indicates that the density profile of NaCl solution is very similar to that of pure water. In light of the interpretation of the XRS spectrum, this is not surprising since only weakening of H-bonds through the hydration of NaCl is observed in XRS. It has been found that the Ornstein–Zernike correlation length of liquid water is reduced significantly by the presence of NaCl salts at supercooled temperatures,[54] which is in accordance with NaCl solution exerting a pressure effect. In contrast, both $MgCl_2$ [Fig. 3(b)] and $AlCl_3$

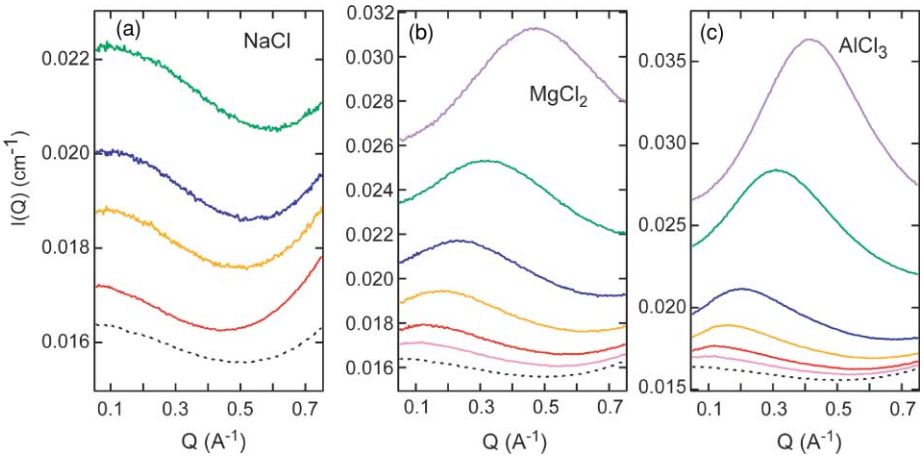

FIG. 3. SAXS data of (a) NaCl, (b) $MgCl_2$, and (c) $AlCl_3$ solutions compared with pure water (black dashes). The solution concentrations from top to bottom are: 1 M, 0.5 M, 0.25 M, 0.1 M for NaCl; 1 M, 0.5 M, 0.25 M, 0.13 M, 0.06 M, 0.03 M for $MgCl_2$; and 0.5 M, 0.25 M, 0.08 M, 0.04 M, 0.019 M, 0.0095 M for $AlCl_3$.

[Fig. 3(c)] solution scattering is dominated by the development of a "prepeak" in the intermediate Q region, i.e., the peak located before the first scattering maximum where the latter is related to the nearest-neighbor distance in the system. Similar prepeaks have been observed in concentrated aqueous solutions[72,73] and melted salts[74] and determined to be largely due to the correlation between cations. The contribution from anion–anion and cation–anion correlations can be neglected in $MgCl_2$ and $AlCl_3$ solutions as indicated by the absence of prepeaks in the case of NaCl solution even up to a high concentration of 2 M (not shown).

Figure 4 compares the SAXS data of NaCl, $MgCl_2$, and $AlCl_3$ at the same concentration with data for bulk water to emphasize the intensity enhancement caused by the multivalent cations. The prepeak position is related to the distance between solvated cations. The shift of the prepeak to higher Q with increasing concentration suggests that the distance between solvated cations decreases as concentration increases. The Q offset between the $MgCl_2$ and $AlCl_3$ prepeaks at the same concentration is attributable to their different widths. More specifically, the narrower $AlCl_3$ peak is less affected by the slowly increased small angle scattering signal and is, therefore, more reliable for the cation–cation distance estimation. A more detailed discussion can be found in the supplementary material.[75]

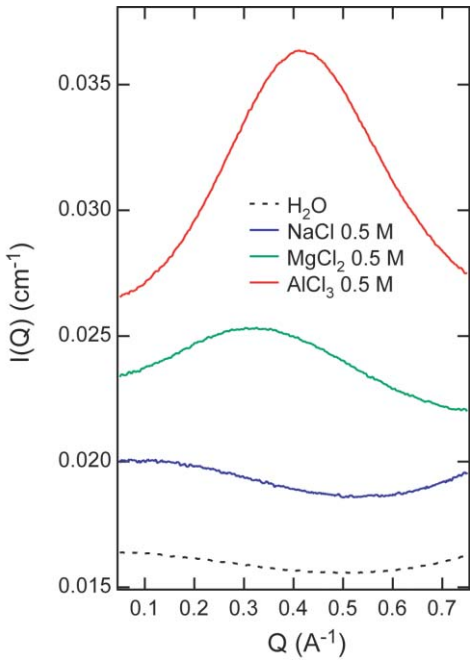

FIG. 4. SAXS data of 0.5 M NaCl (blue), $MgCl_2$ (green), and $AlCl_3$ (red) compared with pure water (black dashes).

Apart from the prepeaks, $MgCl_2$ and $AlCl_3$ solutions show much larger scattering signals at low Q compared to pure water and NaCl solution. We hypothesize that the enhanced low-Q scattering signals are attributable to the presence of well-defined H-bonded shells around hydrated multivalent cations with different local density compared to bulk water. Our hypothesis is consistent with the observation of strongly H-bonded water molecules near the Mg^{2+} and Al^{3+} ions as shown in the XRS spectra (Fig. 1). In the following, we perform a more detailed analysis of the $MgCl_2$ and $AlCl_3$ SAXS data, which can reveal important information about the hydration shells of Mg^{2+} and Al^{3+} cations.

In Fig. 5, the dashed curves were obtained by subtracting the water contribution from the scattering signal of each solution and normalizing each subtracted curve with the concentration. This is done under the assumption that the water molecules outside the hydration shell, including those near the anions, have similar H-bonding environment as in bulk water. The scattering at higher Q overlaps very well within statistical errors and the scattering deviates at $Q < 0.5$ Å^{-1} to a degree depending upon the concentration. The form factor of one individual structure unit (i.e., cation with hydration shells) is then derived by fitting the scattering for the most dilute solution (0.03 M for $MgCl_2$ and 0.0095 M for $AlCl_3$) from the peak maxima to the high Q limit (solid black line). The Cl^- anion is assumed to have a negligible contribution. The measured deviations from the SAXS form factor of solvated cations are indicative of repulsive interactions between them. As the salt concentration increases, the repulsion magnifies resulting in a larger deviation.

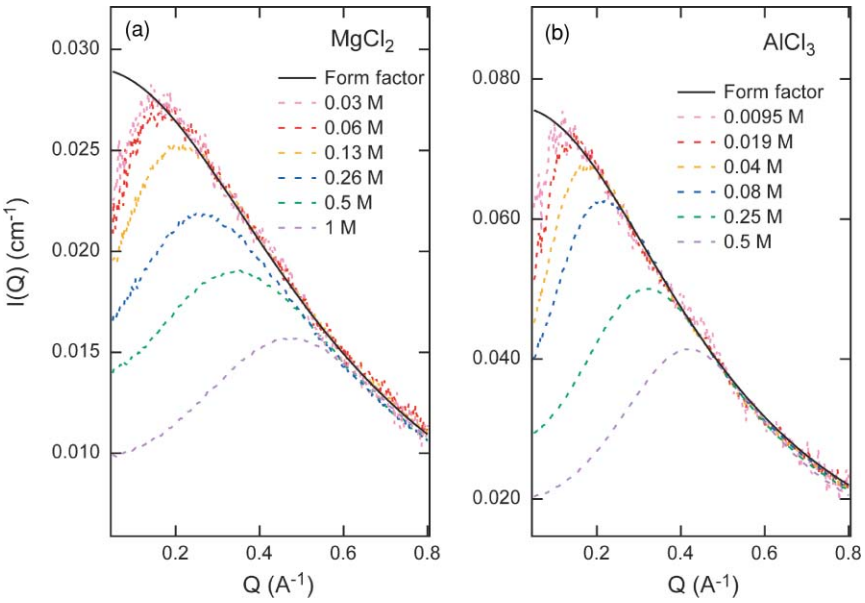

FIG. 5. Dashed curves show the SAXS of $MgCl_2$ (a) and $AlCl_3$ (b) after subtraction of pure water scattering and normalization with concentration. Solid black curves are the form factors obtained by fitting the curve of the most dilute solution (0.03 M for $MgCl_2$ and 0.0095 M for $AlCl_3$) from the prepeak maximum to the high Q limit and extrapolating to $Q = 0$.

In Fig. 6, the form factors of solvated Mg^{2+} and Al^{3+} from experimental data are compared with calculated form factors of Mg^{2+} and Al^{3+} with one and two hydration shells (six water molecules in the first shell and 12 in the second), obtained from the Debye scattering equation:[76]

$$I(Q) = \sum_{m=1}^{N}\sum_{n=1}^{N} f_m(Q) f_n(Q) \frac{\sin Qr_{mn}}{Qr_{mn}}, \tag{1}$$

where N is the number of atoms, $f_m(Q)$ and $f_n(Q)$ are the atomic scattering factors of atoms m and n, and r_{mn} is the distance between atoms m and n. The atomic scattering factor f is calculated using the analytic expression

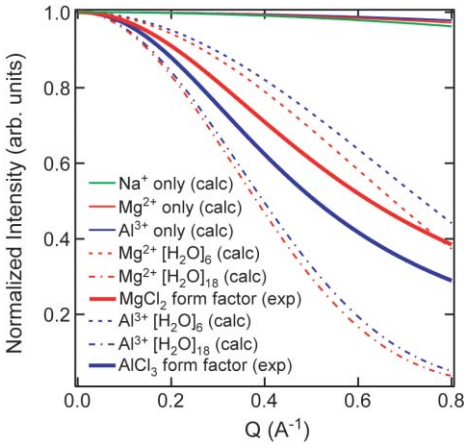

FIG. 6. Comparison of the experimentally determined form factors (thick solid lines) from Fig. 5 with calculated form factors of the cations with one (dashed lines) and two hydration shells (dotted-dashed lines) obtained from the Debye scattering equation. All red lines are for $MgCl_2$ and all blue lines are for $AlCl_3$. The form factors of only the cations are shown as thin solid lines at the top of the figure.

$$f(\lambda^{-1}\sin\theta) = \sum_{i=1}^{4} a_i \exp(-b_i\lambda^{-2}\sin^2\theta) + c, \tag{2}$$

where a_i, b_i, and c are coefficients from Ref. 77 and $\lambda^{-1}\sin\theta = Q/4\pi$. For oxygen and hydrogen, a modification of the atomic scattering factor was introduced as a correction for the covalent bonding in a water molecule, according to Ref. 78,

$$f'(Q) = \left[1 + \alpha \exp\left(\frac{-Q^2}{2\delta^2}\right)\right] f(Q), \tag{3}$$

where $f'(Q)$ is the modified atomic scattering factor, α is the scaling factor for charge redistribution [0.15 for O and −0.6 for H (Ref. 79)], and δ is a parameter for the delocalization of electrons due to chemical bonding [2.2 $Å^{-1}$ (Ref. 78)].

For comparison, the form factors of the cations only (Na^+, Mg^{2+}, and Al^{3+}) are displayed as the thin solid lines at the top of Fig. 6. It is evident that the cations alone cannot account for the experimental form factor of solvated cations in these solutions and their hydration shell(s) must thus play an important role in the scattering. The experimental form factor of solvated Mg^{2+} is close to the calculated form factor of Mg^{2+} with one hydration shell, while the form factor of solvated Al^{3+} is located in between the calculated form factors of Al^{3+} with one and two hydration shells. As a first approximation, the solvated cation structures can be simplified as a homogeneous sphere and its scattering intensity described by the sphere radius R,[80]

$$P(Q) = \left[\frac{3}{(QR)^3}\right]^2 [\sin(QR) - QR\cos(QR)]^2. \tag{4}$$

Fitting the experimental data yields a radius of ∼2.71 and ∼3.18 Å for solvated Mg^{2+} and Al^{3+}, respectively. These numbers are consistent with the radius of an Mg^{2+} cation with one hydration shell and Al^{3+} with 1.5 hydration shells, in agreement with the comparison in Fig. 6. These values reflect

the density contrast given by the hydration shells of Mg^{2+} and Al^{3+} and are not necessarily associated with the actual number of hydration shells of the cations. For both cations, it can, however, be clearly concluded that the water in the first hydration shell represents a different local density from bulk water. For Mg^{2+}, the density of water in the second hydration shell becomes very similar to that of bulk water and the second shell consequently does not appear as a density contrast in SAXS in spite of it being quite strongly H-bonded to the first hydration shell (O–O distance of ~2.71 versus 2.8 Å in bulk water[1,68,69]). Water in the second hydration shell of Al^{3+}, however, can be considered as giving a local density that is between that of the first shell water and bulk water, with an even stronger H-bonding to the first hydration shell compared to Mg^{2+} [O–O distance of ~2.66 Å (Ref. 1, 66–69)].

From the SAXS data, we can also estimate the electron density difference between the solvated ions and the surrounding water molecules using the expression,

$$I(Q=0) = r_0^2 n \Delta\rho^2 v^2, \tag{5}$$

where $I(Q=0)$ is the scattering intensity at $Q=0$ (0.00084 cm^{-1} for Mg^{2+} and 0.00072 cm^{-1} for Al^{3+}), r_0 is the Thomson radius of an electron (2.82×10^{-13} cm), n is the number density of solvated cations, $\Delta\rho$ is the electron density difference between solvated cations and the surrounding bulk water, and v is the volume of the solvated cations from the radius R determined through Eq. (4). Equation (5) yields $\Delta\rho$ of 2.95×10^{23} cm^{-3} for Al^{3+} and 2.90×10^{23} cm^{-3} for Mg^{2+}. Compared to the electron density of pure water ($\rho_{(H_2O)_{bulk}} = 3.31 \times 10^{23}$ cm^{-3}), these values represent an increase of ~88 ± 1% in electron density for the unit structure consisting of the cation and hydration shell(s).

We can then roughly estimate the local density given by water in the hydration shells $\rho_{(H_2O)_{hyd}}$ using

$$\rho_{tot} = \frac{V_{ion}}{V_{tot}}\rho_{ion} + \frac{(V_{tot} - V_{ion})}{V_{tot}}\rho_{(H_2O)_{hyd}}, \tag{6}$$

where $\rho_{tot} = \Delta\rho + \rho_{(H_2O)_{bulk}}$ and ρ_{ion} is the electron density of the cation ($\rho_{ion} = 10$ electrons/V_{ion}). V_{ion} is the volume occupied by the cation in the ion-hydration shell structure, estimated using one half of the cation-oxygen distance as the radius ($d_{Al-O} = 1.9$ Å → $r_{Al^{3+}} = 0.95$ Å, and $d_{Mg-O} = 2.1$ Å → $r_{Mg^{2+}} = 1.05$ Å) and V_{tot} is the volume of the entire ion-hydration shell structure from the radius previously determined using Eq. (4) ($R_{Mg^{2+}+shell} = 2.71$ Å and $R_{Al^{3+}+shell} = 3.18$ Å). From Eq. (6), the electron density of water in the hydration shells is estimated to be 5.65×10^{23} cm^{-3} for Al^{3+} and 5.32×10^{23} cm^{-3} for Mg^{2+}, reflecting ~71% and ~61% increase of electron density from bulk water. Although these numbers seem large, we must consider how water molecules are arranged in the first hydration shell of the cations compared to bulk water. In ice (Fig. 7, right), four water molecules are H-bonded to a central water molecule with O–O distance of 2.75 Å; in liquid water, the O–O distance is even longer (an average of ~2.8 Å) and the H-bonding network fluctuates between tetrahedral and disordered.[45,52] However, around Mg^{2+} and Al^{3+} (Fig. 7, left), six water molecules are arranged in an octahedral geometry with Mg^{2+}–O distance of 2.1 Å and Al^{3+}–O distance of 1.9 Å (Ref. 1). Therefore, in Mg^{2+} and Al^{3+} hydration shells, more water molecules are packed in a smaller volume compared to bulk water, which explains the large increase in electron density.

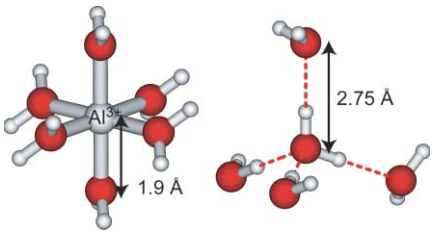

FIG. 7. Depiction of the arrangement of water molecules in: (left) the first hydration shell of Al^{3+} ion, and (right) tetrahedral network in ice.

Although an increase of electron density also suggests an increase in molecular density, we should emphasize here that this is different from the HDL species in bulk water or NaCl solution. The HDL classification in bulk water and NaCl solution is based on a disordered H-bonding network resulting in a more compact structure compared to the LDL species, in which the ordered tetrahedral H-bonding network leaves interstitial spaces resulting in a lower local density. In the case of water in a cation hydration shell, it was discussed above based on the XRS spectra that the water H-bonds between the first and second hydration shells are shorter than those in bulk water, confirming the result of various diffraction studies and molecular dynamics simulations.[1,66–69] In combination with the short cation–oxygen distance, this allows a higher density of ordered water molecules to be present in the hydration shells without introducing interstitial spaces such as those found in LDL water and ice. In addition, whereas the proposed LDL and HDL species in bulk water should continuously interconvert,[45,52] the hydration shells of Mg^{2+} and Al^{3+} are stable on a long time scale albeit with exchange of water molecules occurring.

Our interpretation of the SAXS data is supported by the residence time of water molecules in hydration shells, which is another aspect of ion hydration related to the relative strength of hydration shells. Nuclear magnetic resonance (NMR), quasielastic neutron scattering, and molecular dynamics studies have determined the lifetime of a water molecule in the hydration shells of various cations.[1] Although the exact numbers vary, most studies agree that the residence time of water in the first hydration shell is ~10^{-12} s for Na^+, ~10^{-6} s for Mg^{2+} and 1–6 s for Al^{3+}.[1,67,81] Therefore, the weak hydration shell around Na^+ allows water molecules in the first hydration shell to exchange with those outside the hydration shell on a time scale comparable to H-bond breaking and reforming in bulk water. However, the structures formed by Mg^{2+} and Al^{3+} are relatively stable, and the strongly bound first hydration shell appears as a density contrast in the SAXS data; thus, the exchange of water molecules between the first and second hydration shells occurs much more slowly, particularly for Al^{3+}. The residence time of the water molecules in the second hydration shell of cations is not well known; however, from molecular dynamics simulations it has

been suggested to be on a picosecond time scale for Al^{3+}.[67] In addition, a ^{17}O NMR study has determined the lifetime of the second hydration shell of Cr^{3+} ion as 128 ps.[82] Since the first-shell lifetime of Cr^{3+} is 5 orders of magnitude longer than that of Al^{3+} and 11 orders of magnitude longer than that of Mg^{2+},[1] the lifetime of the second shell of Al^{3+} is expected to be much shorter than 128 ps and for Mg^{2+} it should be even closer to the value for water H-bond breaking and reforming. This indicates that the second shell water molecules of Al^{3+} are more stable than those of Mg^{2+}, although much more mobile than those in the first hydration shell of both cations. In connection to our SAXS data, this indicates that the density of the second hydration shell is very similar to the density of bulk water for Mg^{2+} and in between the densities of bulk water and first hydration shell water for Al^{3+}. This is what we observe in Fig. 6, where Mg^{2+} and Al^{3+} appear to have one and one and a half hydration shells, respectively.

Therefore, half a hydration shell from SAXS data can be interpreted as a gradual change in density between bulk water and the hydration shell instead of an abrupt change. The first hydration shell of both Mg^{2+} and Al^{3+} with six water molecules in an octahedral geometry and relatively short cation–oxygen distance can be considered as having a high-density contrast compared to bulk water. The second hydration shell of Mg^{2+}, although quite strongly bonded to the first hydration shell water molecules, has a similar density to bulk water, and, therefore, in SAXS we only observe one hydration shell around Mg^{2+}. On the other hand, the second hydration shell of Al^{3+} is more stable and rigid compared to that of Mg^{2+} and has a density that is intermediate between bulk water and the first hydration shell which makes it appear in SAXS as half a hydration shell.

IV. CONCLUSIONS

We observe from XRS and SAXS the difference in the way water molecules are structured around Na^+, Mg^{2+}, and Al^{3+}. First, we confirm the FY-XAS study of Näslund *et al.* [40] that cations cause restructuring of the water molecules in their vicinity while anions have a negligible effect. In NaCl solutions, XRS spectra show a weakening of H-bonds corresponding to a conversion from LDL to HDL due to the presence of Na^+; this is similar to the effect of a temperature increase but without inducing increased disorder in the HDL species. The increase in the fraction of HDL species is also consistent with the effect of an increased pressure, supporting the results of Mancinelli *et al.*[16] In contrast, the XRS spectra of $MgCl_2$ and $AlCl_3$ unambiguously show the presence of short H-bonds among water molecules in the vicinity of Mg^{2+} and Al^{3+} ions in agreement with the relatively short O–O distance between water molecules in the first and second hydration shells of Mg^{2+} and Al^{3+} compared to bulk water from various diffraction and simulation studies.[1,66–69]

The SAXS data of NaCl closely resemble that of bulk water indicating that no structures that give an additional density contrast are formed. The scattering curves for $MgCl_2$ and $AlCl_3$, on the other hand, show strongly enhanced signals at low Q and prepeaks at intermediate Q regions arising from structures formed by the cations and water in the hydration shells. Further analysis of the form factors reveals that these structures have a radius of ~2.71 Å for Mg^{2+} and ~3.18 Å for Al^{3+}, corresponding to one and one and a half hydration shells for Mg^{2+} and Al^{3+}, respectively. Electron density estimations suggest that there is ~61% and ~71% increase in electron density in the hydration shells of Mg^{2+} and Al^{3+} compared to bulk water. This is due to the more compact structure of the hydration shells with six water molecules in the first shell and a cation–oxygen distance of ~2.1 Å for Mg^{2+} and ~1.9 Å for Al^{3+} (Ref. 1), compared to the average O–O distance of ~2.8 Å in bulk water. The first hydration shells of both Mg^{2+} and Al^{3+} have completely different density from bulk water. The second hydration shell of Mg^{2+} is very similar to bulk water and is, therefore, invisible to SAXS, while the second hydration shell of Al^{3+} has a density that is intermediate between that of the first hydration shell and bulk water and, therefore, appears as half a hydration shell in SAXS. In summary, from a combination of XRS and SAXS experimental results, we observed that while Na^+ weakens H-bonds in water, Mg^{2+} and Al^{3+} strengthen them by forming stable, highly ordered, high-density hydration shells.

ACKNOWLEDGMENTS

This work was supported by the National Science Foundation (US) CHE-0809324 and the Swedish Research Council. Portions of this research were carried out at the Stanford Synchrotron Radiation Lightsource, a national user facility operated by Stanford University on behalf of the U.S. Department of Energy, Office of Basic Energy Sciences. The BioSAXS beamline 4-2 and the SSRL Structural Molecular Biology Program is supported by the Department of Energy, Office of Biological and Environmental Research, and by the National Institutes of Health, National Center for Research Resources, Biomedical Technology Program.

[1] H. Ohtaki and T. Radnai, Chem. Rev. **93**, 1157 (1993).
[2] Y. Marcus, Chem. Rev. **109**, 1346 (2009).
[3] P. Jungwirth and D. J. Tobias, Chem. Rev. **106**, 1259 (2006).
[4] S. Ghosal, J. C. Hemminger, H. Bluhm, B. S. Mun, E. L. D. Hebenstreit, G. Ketteler, D. F. Ogletree, F. G. Requejo, and M. Salmerón, Science **307**, 563 (2005).
[5] F. Hofmeister, Arch. Exp. Path. Pharmakol. **24**, 247 (1888).
[6] K. D. Collins, Proc. Natl. Acad. Sci. U.S.A. **92**, 5553 (1995).
[7] B. Hribar, N. T. Southall, V. Vlachy, and K. A. Dill, J. Am. Chem. Soc. **124**, 12302 (2002).
[8] G. Jones and M. Dole, J. Am. Chem. Soc. **51**, 2950 (1929).
[9] H. D. B. Jenkins and Y. Marcus, Chem. Rev. **95**, 2695 (1995).
[10] G. A. Krestov and E. R. Myasnikov, *Thermodynamics of Solvation: Solution and Dissolution, Ions and Solvents, Structure and Energetic; Ellis Horwood Series in Physical Chemistry* (Ellis Horwood, New York, 1990).
[11] M. Y. Kiriukhin and K. D. Collins, Biophys. Chem. **99**, 155 (2002).
[12] R. MacKinnon, Angew. Chemie Int. Ed. **43**, 4265 (2004).
[13] Y. F. Zhou, J. H. Morais-Cabral, A. Kaufman, and R. MacKinnon, Nature **414**, 43 (2001).
[14] P. C. Biggin, G. R. Smith, I. Shrivastava, S. Choe, and M. S. P. Sansom, Biochim. Biophys. Acta **1510**, 1 (2001).
[15] S. Y. Noskov and B. Roux, Biophys. Chem. **124**, 279 (2006).
[16] R. Mancinelli, A. Botti, F. Bruni, M. A. Ricci, and A. K. Soper, Phys. Chem. Chem. Phys. **9**, 2959 (2007).
[17] K. T. Wikfeldt, M. Leetmaa, M. P. Ljungberg, A. Nilsson, and L. G. M. Pettersson, J. Phys. Chem. B **113**, 6246 (2009).

[18] J. Holzmann, R. Ludwig, A. Geiger, and D. Paschek, Angew. Chem., Int. Ed. **46**, 8907 (2007).
[19] A. W. Omta, M. F. Kropman, S. Woutersen, and H. J. Bakker, J. Chem. Phys. **119**, 12457 (2003).
[20] A. W. Omta, M. F. Kropman, S. Woutersen, and H. J. Bakker, Science **301**, 347 (2003).
[21] K. J. Tielrooij, N. Garcia-Araez, M. Bonn, and H. J. Bakker, Science **328**, 1006 (2010).
[22] P. A. Bergström, J. Lindgren, M. Read, and M. Sandström, J. Phys. Chem. **95**, 7650 (1991).
[23] J. Stangret and T. Gampe, J. Phys. Chem. A **106**, 5393 (2002).
[24] S. Myneni, Y. Luo, L. Å Näslund, M. Cavalleri, L. Ojamäe, H. Ogasawara, A. Pelmenschikov, Ph. Wernet, P. Väterlein, C. Heske, Z. Hussain, L. G. M. Pettersson, and A. Nilsson, J. Phys.: Condens. Matter **14**, L213 (2002).
[25] M. Cavalleri, H. Ogasawara, L. G. M. Pettersson, and A. Nilsson, Chem. Phys. Lett. **364**, 363 (2002).
[26] Ph. Wernet, D. Nordlund, U. Bergmann, M. Cavalleri, M. Odelius, H. Ogasawara, L. Å. Näslund, T. K. Hirsch, L. Ojamäe, P. Glatzel, L. G. M. Pettersson, and A. Nilsson, Science **304**, 995 (2004).
[27] A. Nilsson, D. Nordlund, I. Waluyo, N. Huang, H. Ogasawara, S. Kaya, U. Bergmann, L. Å. Näslund, H. Öström, Ph. Wernet, K. J. Andersson, T. Schiros, and L. G. M. Pettersson, J. Electron Spectrosc. Relat. Phenom. **177**, 99 (2010).
[28] D. Nordlund, H. Ogasawara, K. J. Andersson, M. Tatarkhanov, M. Salmerón, L. G. M. Pettersson, and A. Nilsson, Phys. Rev. B **80**, 233404 (2009).
[29] M. Leetmaa, M. P. Ljungberg, A. Lyubartsev, A. Nilsson, and L. G. M. Pettersson, J. Electron Spectrosc. Relat. Phenom. **177**, 135 (2010).
[30] M. Odelius, M. Cavalleri, A. Nilsson, and L. G. M. Pettersson, Phys. Rev. B **73**, 024205 (2006).
[31] D. Prendergast and G. Galli, Phys. Rev. Lett. **96**, 215502 (2006).
[32] B. Hetényi, F. De Angelis, P. Giannozzi, and R. Car, J. Chem. Phys. **120**, 8632 (2004).
[33] R. L. C. Wang, H. J. Kreuzer, and M. Grunze, Phys. Chem. Chem. Phys. **8**, 4744 (2006).
[34] M. Cavalleri, M. Odelius, D. Nordlund, A. Nilsson, and L. G. M. Pettersson, Phys. Chem. Chem. Phys. **7**, 2854 (2005).
[35] W. Chen, X. Wu, and R. Car, Phys. Rev. Lett. **105**, 017802 (2010).
[36] E. F. Aziz, M. H. Rittmann-Frank, K. M. Lange, S. Bonhommeau, and M. Chergui, Nature Chem. **2**, 853 (2010).
[37] E. F. Aziz, J. Electron Spectrosc. Relat. Phenom. **177**, 168 (2010).
[38] C. D. Cappa, J. D. Smith, K. R. Wilson, B. M. Messer, M. K. Gilles, R. C. Cohen, and R. J. Saykally, J. Phys. Chem. B **109**, 7046 (2005).
[39] C. D. Cappa, J. D. Smith, B. M. Messer, R. C. Cohen, and R. J. Saykally, J. Phys. Chem. B **110**, 5301 (2006).
[40] L. Å. Näslund, D. C. Edwards, Ph. Wernet, U. Bergmann, H. Ogasawara, L. G. M. Pettersson, S. Myneni, and A. Nilsson, J. Phys. Chem. A **109**, 5995 (2005).
[41] I. Waluyo *et al.* (unpublished data).
[42] Y. Mizuno and Y. Ohmura, J. Phys. Soc. Jpn **22**, 445 (1967).
[43] K. Tohji and Y. Udagawa, Phys. Rev. B **39**, 7590 (1989).
[44] U. Bergmann, Ph. Wernet, P. Glatzel, M. Cavalleri, L. G. M. Pettersson, A. Nilsson, and S. P. Cramer, Phys. Rev. B **66**, 092107 (2002).
[45] C. Huang, K. T. Wikfeldt, T. Tokushima, D. Nordlund, Y. Harada, U. Bergmann, M. Niebuhr, T. M. Weiss, Y. Horikawa, M. Leetmaa, M. P. Ljungberg, O. Takahashi, A. Lenz, L. Ojamäe, A. P. Lyubartsev, S. Shin, L. G. M. Pettersson, and A. Nilsson, Proc. Natl. Acad. Sci. U.S.A. **106**, 15214 (2009).
[46] Ph. Wernet, D. Testemale, J. L. Hazemann, R. Argoud, P. Glatzel, L. G. M. Pettersson, A. Nilsson, and U. Bergmann, J. Chem. Phys. **123**, 154503 (2005).
[47] U. Bergmann, D. Nordlund, Ph. Wernet, M. Odelius, L. G. M. Pettersson, and A. Nilsson, Phys. Rev. B **76**, 024202 (2007).
[48] I. Waluyo, D. Nordlund, U. Bergmann, L. G. M. Pettersson, and A. Nilsson, J. Chem. Phys. **131**, 031103 (2009).
[49] M. H. J. Koch, P. Vachette, and D. I. Svergun, Q. Rev. Biophys. **36**, 147 (2003).
[50] T. Tokushima, Y. Harada, O. Takahashi, Y. Senba, H. Ohashi, L. G. M. Pettersson, A. Nilsson, and S. Shin, Chem. Phys. Lett. **460**, 387 (2008).
[51] A. K. Soper, J. Teixeira, and T. Head-Gordon, Proc. Natl. Acad. Sci. U.S.A. **107**, E44 (2010).
[52] C. Huang, K. T. Wikfeldt, T. Tokushima, D. Nordlund, Y. Harada, U. Bergmann, M. Niebuhr, T. M. Weiss, Y. Horikawa, M. Leetmaa, M. P. Ljungberg, O. Takahashi, A. Lenz, L. Ojamäe, A. P. Lyubartsev, S. Shin, L. G. M. Pettersson, and A. Nilsson, Proc. Natl. Acad. Sci. U.S.A. **107**, E45 (2010).
[53] G. N. I. Clark, G. L. Hura, J. Teixeira, A. K. Soper, and T. Head-Gordon, Proc. Natl. Acad. Sci. U.S.A. **107**, 14003 (2010).
[54] C. Huang, T. M. Weiss, D. Nordlund, K. T. Wikfeldt, L. G. M. Pettersson, and A. Nilsson, J. Chem. Phys. **133**, 134504 (2010).
[55] J. Stöhr, *NEXAFS Spectroscopy* (Springer, Berlin, 1991).
[56] F. Sette, J. Stöhr, and A. P. Hitchcock, Chem. Phys. Lett. **110**, 517 (1984).
[57] J. Stöhr, J. L. Gland, W. Eberhardt, D. Outka, R. J. Madix, F. Sette, R. J. Koestner, and U. Doebler, Phys. Rev. Lett. **51**, 2414 (1983).
[58] M. N. Piancastelli, D. W. Lindle, T. A. Ferrett, and D. A. Shirley, J. Chem. Phys. **86**, 2765 (1987).
[59] C. Puglia, A. Nilsson, B. Hernnäs, O. Karis, P. Bennich, and N. Mårtensson, Surf. Sci. **342**, 171 (1995).
[60] N. Haack, G. Ceballos, H. Wende, K. Baberschke, D. Arvanitis, A. L. Ankudinov, and J. J. Rehr, Phys. Rev. Lett. **84**, 614 (2000).
[61] A. Nilsson, H. Ogasawara, M. Cavalleri, D. Nordlund, M. Nyberg, Ph. Wernet, and L. G. M. Pettersson, J. Chem. Phys. **122**, 154505 (2005).
[62] M. Cavalleri, L. Å. Näslund, D. C. Edwards, Ph. Wernet, H. Ogasawara, S. Myneni, L. Ojamäe, M. Odelius, A. Nilsson, and L. G. M. Pettersson, J. Chem. Phys. **124**, 194508 (2006).
[63] L. Å. Näslund, M. Cavalleri, H. Ogasawara, A. Nilsson, L. G. M. Pettersson, Ph. Wernet, D. C. Edwards, M. Sandström, and S. Myneni, J. Phys. Chem. A **107**, 6869 (2003).
[64] H. Ogasawara, B. Brena, D. Nordlund, M. Nyberg, A. Pelmenschikov, L. G. M. Pettersson, and A. Nilsson, Phys. Rev. Lett. **89**, 276102 (2002).
[65] R. Mancinelli, A. Botti, F. Bruni, M. A. Ricci, and A. K. Soper, J. Phys. Chem. B **111**, 13570 (2007).
[66] T. M. C. Faro, G. P. Thim, and M. S. Skaf, J. Chem. Phys. **132**, 114509 (2010).
[67] E. J. Bylaska, M. Valiev, J. R. Rustad, and J. H. Weare, J. Chem. Phys. **126**, 104505 (2007).
[68] D. Spångberg and K. Hermansson, J. Chem. Phys. **120**, 4829 (2004).
[69] J. M. Martinez, R. R. Pappalardo, and E. S. Marcos, J. Am. Chem. Soc. **121**, 3175 (1999).
[70] E. F. Aziz, A. Zimina, M. Freiwald, S. Eisebitt, and W. Eberhardt, J. Chem. Phys. **124**, 114502 (2006).
[71] E. F. Aziz, N. Ottosson, S. Eisebitt, W. Eberhardt, B. Jagoda-Cwiklik, R. Vacha, P. Jungwirth, and B. Winter, J. Phys. Chem. B **112**, 12567 (2008).
[72] G. W. Neilson, R. A. Howe, and J. E. Enderby, Chem. Phys. Lett. **33**, 284 (1975).
[73] R. Caminiti and M. Magini, Chem. Phys. Lett. **54**, 600 (1978).
[74] K. F. Ludwig, L. Wilson, W. K. Warburton, and A. I. Bienenstock, J. Chem. Phys. **87**, 613 (1987).
[75] See supplementary material at http://dx.doi.org/10.1063/1.3533958 for a detailed description of the cation–cation distance from the SAXS data.
[76] B. E. Warren, *X-ray Diffraction* (Dover, New York, 1990).
[77] D. T. Cromer and J. T. Waber, "Atomic scattering factors for x-rays," in *International Tables for X-Ray Crystallography*, Vol. 4, edited by J. A. Ibers and W. C. Hamilton (Kynoch, Birmingham, 1974).
[78] J. M. Sorenson, G. Hura, R. M. Glaeser, and T. Head-Gordon, J. Chem. Phys. **113**, 9149 (2000).
[79] L. Fu, A. Bienenstock, and S. Brennan, J. Chem. Phys. **131**, 234702 (2009).
[80] G. Grubel and F. Zontone, J. Alloys Compd. **362**, 3 (2004).
[81] S. Koneshan, J. C. Rasaiah, R. M. Lynden-Bell, and S. H. Lee, J. Phys. Chem. B **102**, 4193 (1998).
[82] A. Bleuzen, F. Foglia, E. Furet, L. Helm, A. E. Merbach, and J. Weber, J. Am. Chem. Soc. **118**, 12777 (1996).